Circulation: Arrhythmia and Electrophysiology

ORIGINAL ARTICLE

Heart Digital Twins Predict Features of Invasive Reentrant Circuits and Ablation Lesions in Scar-Dependent Ventricular Tachycardia

Michael C. Waight; MBBS, BSc(Hons), MRCP; Adityo Prakosa; PhD; Anthony C. Li; MD(Res), MBBS, BSc(Hons), MRCP; Anh Truong; BSc; Nick Bunce; MD, MBBS, BSc, MRCP; Anna Marciniak; MBBS, PhD, MRCP; Natalia A. Trayanova; PhD*; Magdi M Saba; MD, MSc*

BACKGROUND: Catheter ablation of scar-dependent ventricular tachycardia (VT) is frequently hampered by hemodynamic instability, long procedure duration, and high recurrence rates. Magnetic resonance imaging-based personalized heart digital twins may overcome these challenges by noninvasively predicting VT circuits and optimum ablation lesion sites. In this combined clinical and digital twin study, we investigated the relationship between digital twin-predicted VTs and optimum ablation lesion sets with their invasively mapped counterparts during clinical VT ablation.

METHODS: A total of 18 patients with scar-dependent VT underwent digital twin creation based on preprocedural, contrast-enhanced cardiac magnetic resonance imaging. Using rapid pacing protocols, VT was simulated and ablation targets were derived that would terminate all possible VTs in the models. Patients subsequently underwent invasive VT ablation, including targeting of diastolic activity and optimum entrainment sites. Digital twin-predicted VT circuits and ablation lesions were compared with their invasive clinical counterparts.

RESULTS: Forty-three clinical VTs and 92 digital twin VTs were induced. Diastolic activity was seen in 16 of 43 (37.2%) clinical VTs. Sensitivity, specificity, positive predictive, and negative predictive values for the detection of critical VT sites by digital twins were 81.3%, 83.8%, 21.7%, and 98.8%, respectively. At an AHA-segment level, agreement between clinical VT critical sites and digital twin primary predicted sites was moderate, with a κ coefficient of 0.46 (±0.32; $P \leq 0.001$). Termination of VT with ablation was achieved at a digital twin-predicted site in 4 of 5 (80%) cases where attempted. A total of 426 of 709 (60.1%) lesions were within 5 mm of a predicted target site. In total, 54.0% (±28.9%) of the digital twin-predicted area was ablated per patient based on conventional mapping criteria.

CONCLUSIONS: Heart digital twin VT circuits and ablation targets accurately predict many features of their respective clinical counterparts but have some limitations in spatial resolution. Our findings demonstrate the significant potential of digital twin technology in guiding catheter ablation for scar-dependent VT.

GRAPHIC ABSTRACT: A graphic abstract is available for this article.

Key Words: catheter ablation ■ heart rate ■ humans ■ magnetic resonance imaging ■ technology

Scar-dependent ventricular tachycardia (VT) is a life-threatening arrhythmia that predisposes patients to sudden cardiac death.[1] Catheter ablation therapy, aimed at destroying myocardial tissue that perpetuates the arrhythmia, offers freedom from VT.[2–6] The current gold standard approach for catheter ablation of VT is to

Correspondence to: Michael Waight, MBBS, BSc(Hons), MRCP, St George's University of London, Cranmer Terr, London SW170RE, United Kingdom. Email m2110065@citystgeorges.ac.uk
*N.A. Trayanova and M.M. Saba contributed equally as joint senior coauthors.
Supplemental Material is available at https://www.ahajournals.org/doi/suppl/10.1161/CIRCEP.124.013660.
For Sources of Funding and Disclosures, see page XXX.

Circulation: Arrhythmia and Electrophysiology is available at www.ahajournals.org/journal/circep

WHAT IS KNOWN?

- The current gold standard for ventricular tachycardia catheter ablation includes induction and mapping of ventricular tachycardia (VT) to help guide ablation, a process which is time consuming and potentially risky.
- Heart digital twin technology can noninvasively simulate VT circuits and predict optimum ablation lesion sites to terminate VT in patient-specific models.

WHAT THE STUDY ADDS

- Digital twins can accurately predict the critical VT isthmus including sites of diastolic activity and termination of VT with ablation as well as the final clinical ablation lesion sets delivered during VT ablation.

Nonstandard Abbreviations and Acronyms

EAM	electroanatomical map
ECF	entrainment with concealed fusion
ICM	ischemic cardiomyopathy
LV	left ventricular
MDP	mid-diastolic potential
MRI	magnetic resonance imaging
NICM	nonischemic cardiomyopathy
PES	programmed electrical stimulation
VT	ventricular tachycardia

induce and map the clinical VT and ablate the critical isthmus of the reentrant circuit.[7] Isthmus sites are characterized by surviving channels of viable myocytes through an area of scar tissue and are complex in their architecture, characterized by variations in conduction velocity, tissue anisotropy, and regions of conduction block,[8–10] providing the necessary milieu for reentry to occur. Classical studies have demonstrated the presence of diastolic activity and typical responses to ventricular entrainment during VT at these critical sites,[11,12] which mark them out as optimal ablation targets if observed, and where termination of VT with ablation is frequently achieved.[11,12] In clinical practice, this approach is often impossible due to hemodynamic instability. This limitation, in part, explains the suboptimal outcomes and high recurrence rates observed in large VT ablation trials.[4,5,13,14] Furthermore, VT ablation is time consuming and is associated with a significant risk of complications.[15,16] Therefore, new strategies are required to overcome these limitations and improve outcomes in VT ablation.

One potential strategy to overcome these limitations is the use of medical digital twins to guide catheter ablation. A medical digital twin is a digital replica of a patient or an organ that can be used to study a specific disease process, predict patient trajectories, or develop personalized therapies.[17] In the case of cardiac electrophysiology, there have been recent advances in modeling the electrical functioning of the organ, which have led to the realization of the personalized heart digital twin.[18–23] This noninvasive tool uses cardiac imaging and other data to generate a multiscale heart model that accurately represents a patient's unique cardiac anatomy and electrophysiology. When reconstructed from contrast-enhanced magnetic resonance imaging (MRI), which visualizes the distribution of scar and fibrosis in the heart, these heart digital twins incorporate the mechanistic underpinning of scar-dependent VT. Such heart digital twins have been used to test for arrhythmia inducibility and have been utilized in the prediction of risk of sudden cardiac death.[18,19] Heart digital twins could also predict the optimum personalized lesion sets for ablation of scar-dependent VT, which would terminate all potential VTs in the most efficient manner possible, by identifying the VT isthmus.[19,20,23] If accurate, these digital twin predictions have the potential to substantially reduce procedure time and may guide ablation of not only the clinical VT present in the native scar substrate, but also sites that may result in VT recurrence following an initial ablation procedure.[18,19,24,25] Recently, digital twins have been shown to accurately predict sites of electrogram abnormalities as well as conduction slowing during substrate mapping in patients with VT.[26] However, it is also essential to establish how these digital twin-derived targets compare against the conventional markers of the critical VT isthmus based on invasive activation and entrainment mapping during VT. Furthermore, establishing the relationship between the digital twin-predicted ablation targets and those formed through conventional VT mapping techniques is critical before these digital twin models can be used to guide VT ablation.

Here, we present a prospective, combined digital twin and clinical VT mapping and ablation study to determine the relationship between invasively defined VT circuits and clinical ablation targets and their respective counterparts observed in the digital twins. For the first time, digital twin-derived VT circuits and predicted ablation targets are directly compared with the invasively mapped reentrant VT and clinical ablation lesions during catheter ablation. Establishing this relationship is the foundation required for a future randomized controlled trial directly comparing digital-twin-guided ablation to conventional ablation, with the promise of a radical overhaul in our approach to scar-dependent VT ablation.

METHODS

All patients described in this study provided written, informed consent. The study was approved by the Health Research Authority London—Surrey Research Ethics Committee (21/LO/0083). ClinicalTrials.gov reference number:

REGISTRATION: URL: https://www.clinicaltrials.gov; Unique identifier: NCT04632394. The data supporting the findings of this study are available from the corresponding author upon reasonable request.

Study Overview

Patients requiring catheter ablation for VT were prospectively enrolled into this clinical and digital twin study. Patients underwent 3-dimensional late gadolinium-enhanced cardiac magnetic resonance before the ablation procedure. These images were used to generate digital twin representations, which accurately reflect the unique distribution of scar in each patient. VT inducibility in the personalized digital twins was tested through pacing protocols, and if reentrant arrhythmia was identified, the circuit morphology within the fibrotic milieu was analyzed to ascertain the optimum targets for ablation. Through comprehensive re-testing and application of further lesions to the postablation substrate, the models were rendered noninducible to all VT. Next, patients underwent invasive VT ablation, including VT induction, mapping, and radiofrequency ablation. The characteristics of both the digital twins' and the invasively mapped circuits were analyzed. Markers of the critical VT isthmus, as well as the predicted and invasively delivered radiofrequency lesions, were analyzed, and the overlap between the digital twins and invasive clinical findings was compared. The digital twin modeling and VT ablation procedures were each performed by independent investigators, blinded to the outcomes of the opposite modality. Figure 1 presents a schematic of the study.

Patient Cohort

Inclusion requirements included structural heart disease (either ischemic [ICM] or nonischemic [NICM] cardiomyopathy), documented recurrent VT or Implantable Cardioverter Defibrillator therapy, or prohibitive side effects from antiarrhythmic medications. Patients with insufficient MRI quality were excluded. The patients recruited into this study were the same as in our recent publication.[26]

CMR Image Processing

Three-dimensional late gadolinium-enhanced cardiac magnetic resonance was acquired using either a 3T or 1.5T scanner depending on the presence of cardiac devices. Further details of the image acquisition and digital twin generation are described in previous publications,[19,22] and outlined in the Supplemental Methods. Images were exported and segmented in a semi-automated fashion as described previously[18,19,22] To summarize, landmark control points were placed at various

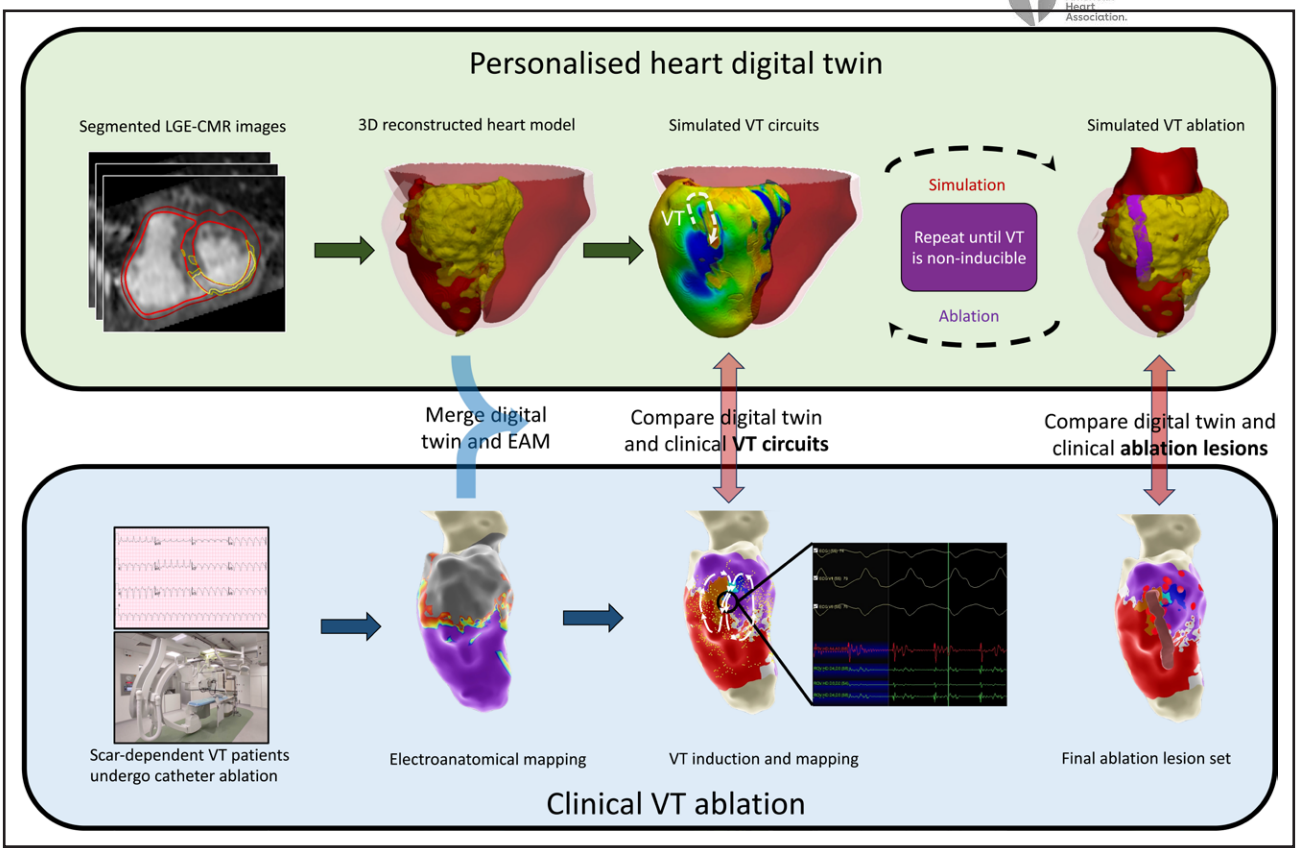

Figure 1. Study overview.
Personalized heart digital twin creation (**top line**): 3-dimensional late gadolinium-enhanced cardiac magnetic resonance (3D LGE-CMR) images are segmented and a personalized heart digital twin created. This model is tested for arrhythmia inducibility and optimum ablation targets to terminate all possible ventricular tachycardias (VTs) in the model. Clinical VT ablation (bottom line): Patients with scar-dependent VT undergo conventional electroanatomical mapping, which is merged with the digital twin. VT is induced and mapped for comparison with digital twin VT simulations. Final clinical ablation lesion set is compared with the digital twin-predicted ablation lesion set. EAM indicates electroanatomical map.

points along the endocardial and epicardial surfaces. Using a variational implicit method[24] the remaining boundaries were automatically defined.

Generation of the Heart Digital Twin

Following segmentation, myocardial tissue was categorized as either healthy tissue, border zone, or dense scar by signal thresholding using the full-width half-maximum approach.[27] Finite-element meshes with an average resolution of ≈400 µm were generated with each mesh containing ≈4 million individual nodes.[28] Fiber directionality was overlaid onto the mesh on a per-element basis using a validated rule-based approach.[29] Tissue characteristics of healthy tissue, border zone and dense scar were superimposed onto this mesh.

Application of Electrophysiological Properties to the Digital Twin

Electrophysiological properties were applied to each of the 3 tissue regions within the mesh. Properties of healthy tissue were modeled with the 10 Tusscher ionic model of the human ventricular myocyte.[30] Modifications to the ionic properties were made in border zone areas, including longer action potential duration and reduced conduction velocity, based on previous experimental models.[31,32] Wavefront propagation was simulated by solving the reaction-diffusion partial differential equation using the open-source software openCARP (https://opencarp.org) using a parallel computing system.[33]

Simulated VT Induction and Ablation Protocol

Simulated pacing was applied sequentially to 7 left ventricular (LV) sites based on a condensed AHA 17-segment model to systematically probe the models for VT inducibility. Pacing was preferentially projected onto the closest area of scar border zone to maximize detection of VT. Pacing was delivered as a train of 6 beats with a cycle length of 600 ms (S1), followed by up to 3 extrastimuli. Reentry was defined as undergoing at least 2 rotational cycles at the same site, as in previous studies.[18–20] Once reentry was confirmed, the VT was manually inspected for components consistent with critical sites including the entrance, isthmus, and exit. Simulated ablation lesions were applied at the VT isthmus by changing the local tissue properties to render that area electrically inert using the smallest volume of ablation possible. The ablation lesion set which terminates the specific VT were termed predicted target sites . Where feasible, ablation lesions were connected to areas of dense scar or anatomic barriers (such as the mitral isthmus) to reduce the chance of iatrogenic reentry following initial ablation set application. Several iterations of the ablation process were run to ensure the most volume-efficient lesion set was applied for a particular VT. Ablation lesions that terminated VTs in the native scar substrate were termed primary target sites. Following the application of all ablation lesions within the native substrate, the VT induction and ablation protocol was repeated in the new substrate (containing both native scar and primary ablation lesions), to assess for emergent VTs that may manifest in the new, modified substrate. Any emergent VTs were targeted for ablation in the digital twin in the same fashion and were labeled secondary target sites. The process was repeated until the model was no longer inducible to VT.[34–36]

Model Integration

Surfaces from the model, including the endocardial and epicardial surfaces, primary and secondary predicted target sites, and fiducial landmarks, were exported for rigid coregistration with the invasive electroanatomic map (EAM) using the Ensite Fusion Registration Module. Coregistration was performed by expert individuals, independent of subsequent analysis and blinded to the predicted target site locations. The clinical operators were blinded to the digital twin model at all times.

Invasive VT Mapping and Ablation Protocol

Antiarrhythmic medications were discontinued 5 half-lives before ablation, with the exception of amiodarone, which was discontinued 1 week before ablation. Ablation was performed under general anesthesia. Epicardial access was gained at the operator's discretion and was utilized particularly in the case of NICM and those presenting for redo ablation. LV access was achieved via both transseptal and retrograde aortic approaches. Electroanatomical mapping was performed with the Advisor HD Grid mapping catheter (Abbott Laboratories, Chicago, IL) using either the Ensite Precision or Ensite X mapping systems.

Following generation of a comprehensive substrate map, patients underwent programmed electrical stimulation (PES) with up to 3 extrastimuli using 2 different drive cycle lengths from the right ventricular apex. If no VT could be induced from the right ventricular apex, a repeat attempt was made from the right ventricular septum or the LV within an area of scar. Significant VTs were defined as those matching the clinical VT (either through 12-lead ECG morphology or similarity in cycle length to VT on Implantable Cardioverter Defibrillator interrogation), or those which were reproducibly induced. VTs with a cycle length of <200 ms, ventricular flutter, and ventricular fibrillation were not targeted.

If VT was hemodynamically stable, it was mapped conventionally,[12] including entrainment mapping where possible at sites of diastolic activity. In the case of poorly tolerated VT, substrate mapping, pacemapping and strategic multielectrode positioning (StaMP mapping) were used to elucidate the critical sites for reentry.

Ablation was targeted to critical sites for reentry, which were defined as:

- ECF, with a postpacing interval within 30 ms of the tachycardia cycle length, a stimulus-to-QRS interval within 10 ms of the EGM-to-QRS interval and stimulus-to-QRS interval within 30% to 70% of the tachycardia cycle length.
- EGMs within or adjacent to a low-voltage region (<1.5 mV) exhibiting mid-diastolic activity (defined as an EGM occurring between 30% and 70% of the ventricular diastolic period) during VT.
- Sites exhibiting termination of tachycardia with ablation.
- >80% pacemap match with stimulus-to-QRS interval >30 ms, evidence of multiple exit sites, or pacemap induction of VT.

In the absence of any of the above features, a substrate-guided approach was taken. Ablation was performed using the TactiCath Sensor Enabled (Abbott Laboratories, Chicago, IL). Ablation was performed at 30 to 50 W targeting 60 seconds per lesion, and an impedance drop of >10Ω, attenuation of abnormal potentials, or until loss of capture during pacing at 10

mA for 2 ms. The procedural end point was defined as noninducibility of all significant VTs following repeat PES.

Predicted Target Site Analysis

Presence of digital twin-predicted VTs and invasively induced VTs was assessed on a 17 AHA-segment basis for each patient and the diagnostic accuracy of the digital twin in detecting mid-diastolic potentials (MDPs), optimum entrainment sites, and sites of VT termination with ablation was established. Agreement between induced clinical VT isthmuses and digital twin primary predicted sites was assessed. The area of predicted ablation targets was compared between ICM and NICM cohorts, and between primary and secondary target sites.

Correlation of Diastolic Activity With Digital Twin-Predicted Target Sites

Areas of diastolic activity during VT were marked on the EAM. The spatial correlation of diastolic activity with predicted target sites was measured. Diastolic activity within 5 mm of a predicted target site, measured as geodesic distance, was considered spatially related to that predicted site. Where possible, termination of VT during radiofrequency ablation was attempted and recorded as a marker of the critical isthmus. The positions of optimum entrainment sites and sites of termination with ablation were spatially compared with the predicted primary and secondary target sites.

Ablation Lesion Analysis

Ablation was performed blinded to the digital twin model and targeted sites deemed critical for reentry, as defined above. The area of clinical ablation was measured on the EAM and compared with the area of the predicted target sites. The overlap between the clinical radiofrequency ablation lesion set and the predicted target sites was calculated. Overlap between the ablation area and the low-voltage area was also calculated. The geodesic distance of each ablation lesion from a predicted target site was calculated.

Statistical Analysis

Continuous, normally distributed data are expressed as means±SD. Nonparametric data are expressed as medians±interquartile range. Categorical data are expressed as a percentage. Agreement between clinically observed and digital twin primary predicted VTs was assessed with the Cohen κ coefficient. The generalized estimating equation method was used to compare predicted site and clinical VT parameters, accounting for repeated measurements from the same individual and controlling for age, sex, etiology, and antiarrhythmic drug use as covariates where appropriate. A P value of <0.05 was taken to indicate statistical significance. Statistical analysis was performed using SPSS, version 30 (IBM Corp, Armonk, NY).

RESULTS

Patient Demographics

A total of 18 patients were recruited into the study. In total, 15 of 18 (83.3%) had ICM and 3 of 18 (16.7%) had NICM. Seventeen of 18 (94.4%) were male. Baseline LV ejection fraction was 42.3% (±16.5%). Epicardial mapping was used in 5 of 18 (27.8%) cases. Overall acute procedural success, defined as noninducibility for any sustained VT, was 88.9%. Procedure duration was 227 (±61) minutes. There was 1 procedure-related complication observed, constituting a late-presenting ventricular septal defect requiring patch repair following ablation at the basal interventricular septum in scar with a wall thickness of 7.0 mm. Table 1 shows the full list of demographic and procedural characteristics for the cohort.

Induced and Digital Twin-Predicted VT Characteristics

During clinical VT ablation, monomorphic VT was inducible in 15 of 18 (83.3%) patients. Two of 18 (11.1%) were not inducible to any ventricular arrhythmia, while 1 of 18 (5.6%) was only inducible for VF. A total of 43 VTs were induced in the cohort. The mean number of clinical VTs induced per patient was 2.4 (range 0–6). Fourteen of 18 (77.8%) patients had at least 1 partially mappable VT.

All 18 heart digital twins of the patients were inducible to VT. Sensitivity and positive predictive value of the digital twin for predicting VT inducibility were 100% and 83.3%, respectively. A total of 92 VTs were predicted, with a mean of 5.3 (range 1–8) VTs predicted per patient. This comprised 3.5 (range 1–6) primary VTs (apparent in the native scar substrate) and 1.7 (range 0–4) secondary VTs (emergent following application of the primary ablation lesion set). We observed a greater number of VTs in the digital twin models than were induced clinically, suggesting the digital twins detect additional VT circuits which may be responsible for VT recurrences. The VT isthmus was predicted to be epicardial as opposed to endocardial in 40/92 (43.5%) of VTs, with a higher proportion of epicardial VTs predicted in the NICM cohort compared with the ICM cohort (10/15 [66.7%] versus 30/77 [38.9%]; P=0.048). The digital twin predictions are thus in keeping with previous clinical studies which show a preponderance of epicardial VT circuits in those with NICM. VT characteristics for the cohort are shown in Table 2.

Predicted Target Site Characteristics

Mean total target area for VT ablation in the digital twins was 10.9 cm^2 (±3.9 cm^2) comprising 7.7 cm^2 (±2.6 cm^2) as primary targets and 3.2 cm^2 (±3.2 cm^2) as secondary targets. The mean area of individual VT targets was smaller in the ICM cohort compared with the NICM cohort (2.04 cm^2 [±0.84 cm^2] versus 2.61 cm^2 [±1.26 cm^2]; P=0.001). Overlap of predicted sites with EAM-defined low bipolar voltage (<1.5 mV) area was 5.9 cm^2 (±2.2 cm^2), comprising 56.8% of the total target area.

Table 1. Demographic and Procedural Characteristics of the Cohort

	ICM (15)	NICM (3)	Total (18)
Age, y	67.7 (±9.7)	71.7 (±7.4)	68.4 (±9.5)
Male gender	14 (93.3%)	3 (100%)	17 (94.4%)
Baseline LVEF (%)	41.5 (±17.7)	46.3 (±10.0)	42.3 (±16.5)
NYHA class			
I	7 (46.6%)	1(33.3%)	8 (44.4%)
II	5 (33.3%)	2 (66.7%)	7 (38.9%)
III	3 (20.0%)	0	3 (16.7%)
IV	0	0	0
Hypertension	11 (73.3%)	2 (66.7%)	13 (72.2%)
Diabetes	6 (40.0%)	1 (33.3%)	7 (38.9%)
Atrial fibrillation	6 (40.0%)	2 (66.7%)	8 (44.4%)
Chronic kidney disease	7 (46.7%)	2 (66.7%)	9 (50.0%)
β-Blocker	14 (93.3%)	3 (100%)	17 (94.4%)
Amiodarone	4 (26.7%)	3 (100%)	7 (38.9%)
Mexiletine	2 (13.3%)	1 (33.3%)	3 (16.7%)
ICD	12 (80.0%)	3 (100%)	15 (83.3%)
CRT-D	2 (10.7%)	0	2 (11.1%)
Prior VT ablation	2 (13.3%)	0	2 (11.1%)
Epicardial mapping	3 (16.7%)	2 (66.7%)	5 (27.8%)
Right ventricular mapping	2 (11.1%)	2 (66.7%)	4 (22.2%)
VA Inducible	13 (86.7%)	3 (100%)	16 (88.9%)
No. of induced VTs (range)	2.5 (range 0–6)	2.0 (range 1–3)	2.4 (range 0–6)
At least 1 mappable VT	11 (73.3%)	3 (100%)	14 (77.8%)
Fastest VT TCL (ms; IQR)	265 (242–290)	286 (259–291)	270 (242–290)
Slowest VT TCL (ms; IQR)	314 (285–369)	314 (292–355)	314 (285–369)
Procedural outcome			
Success	14 (93.3%)	2 (66.7%)	16 (88.9%)
Partial success/ failure	1 (6.7%)	1 (33.3%)	2 (11.1%)
Procedure time, m	213 (±48.5)	283 (±83)	227 (±61)
Number of radiofrequency lesions	38.7 (±20.2)	44.0 (±36.6)	39.6 (±22.3)
Radiofrequency ablation time, m:s	36:46 (±16:54)	32:52 (±22:28)	36:04 (±17:15)
Procedure-related complications	0	1 (33.3%)	1 (6.3%)

CRT-D indicates cardiac resynchronization therapy-defibrillator; ICD, Implantable Cardioverter Defibrillator; ICM, ischemic cardiomyopathy; LVEF, left ventricular ejection fraction; NICM, nonischemic cardiomyopathy; TCL, tachycardia cycle length; and VT, ventricular arrhythmia.

Table 2. Characteristics of Induced and Predicted VTs

	ICM (15)	NICM (3)	Total (18)
VT clinically inducible	12 (80.0%)	3 (100%)	15 (83.3%)
Total induced VTs	37	6	43
VTs per patient (range)	2.5 (range 0–6)	2.0 (range 1–3)	2.4 (range 0–6)
At least 1 mappable VT	11 (73.3%)	3 (100%)	14 (77.8%)
Fastest VT TCL, ms	263 (240–284)	290 (288–291)	270 (246–291)
Slowest VT TCL, ms	310 (284–369)	314 (300–327)	314 (286–360)
Utilized VT mapping points	212 (72–498)	494 (394–668)	220 (88–501)
VTs with MDP detected	13	3	16
Total DT-predicted VTs	77	15	92
DT-predicted VTs per patient (range)	5.3 (1–8)	5 (3–6)	5.3 (1–8)
Primary	3.4 (1–5)	4 (3–6)	3.5 (1–6)
Secondary	1.9 (0–4)	1 (0–3)	1.7 (0–4)
DT-predicted epicardial isthmus	30 (38.9%)	10 (66.7%)	40 (43.5%)

DT indicates digital twin; ICM, ischemic cardiomyopathy; NICM, nonischemic cardiomyopathy; TCL, tachycardia cycle length; and VT, ventricular tachycardia.

However, 9.8 cm^2 (±3.5 cm^2) of predicted target sites lay within CMR-defined scar, comprising 89.9% of the total target area. These findings demonstrate that digital twins accurately predict the VT circuits and their relationship to myocardial scar. There was no significant difference in the size of individual primary isthmus targets compared with secondary isthmus targets (2.25 cm^2 [±0.92 cm^2] versus 1.90 cm^2 [±0.97 cm^2]; P=0.10). The most common location for a predicted target site was mid inferolateral (17.4%), followed by basal inferoseptal (12.0%) and basal inferolateral (10.7%). This was in keeping with the observed MRI scar distribution.

Correlation Between Diastolic Activity During VT and Predicted Target Sites

MDPs, the hallmark of the VT isthmus, were observed in 16 of 43 (37.2%) of VTs. VTs in which an MDP was detected exhibited a greater number of mapping points compared with those where an MDP was not seen (710 [±902] versus 142 [±202]; P=0.02). Tachycardia cycle length of VTs where an MDP was detected was not significantly different from those where an MDP was not detected, (310 ms [±65 ms] versus 283 ms [±39 ms]; P=0.13).

Among the 16 VTs where an MDP was detected, sensitivity of predicted target sites to detecting MDPs was 81.3%, with 13 of 16 MDPs being located within 5 mm of a predicted target site. In the remaining 3 of 16 cases (18.8%), the MDP was remote. Crucially, these results showcase the powerful predictive capability of digital twins for noninvasively detecting the critical components of the VT circuits, and complement the findings from our recent publication, which demonstrated a close alignment of digital twin-predicted sites with zones of slow conduction on isochronal late activation mapping with 80.8% of deceleration zones

being detected by the digital twin-predicted sites.[26] Of the 16 identified VT MDPs, 5 (31.3%) collocated to within 5 mm of one of the previously described deceleration zones. Figure 2 shows an example of a mapped VT involving an inferior wall scar. The VT activation map showed a VT isthmus with MDPs which correlated closely to a predicted target site. Pacing at the site of the isthmus led to a perfect pacemap match. Entrainment at this location led to termination of the tachycardia. Figure 3 shows the same patient's VT which visually corresponded closely to a predicted VT during testing of the digital twin.

Correlation Between Entrainment Sites, VT Termination With Ablation and Predicted Target Sites

Due to poor hemodynamic stability of the majority of induced VTs, entrainment mapping was only attempted in 4 of 16 VTs where an MDP was observed. When performed, entrainment with concealed fusion (ECF) was demonstrated in 3 of 4 cases (75%). Fusion was manifest in 1 of 4 cases (25%). In all 3 cases of ECF, the site of ECF was directly beneath a predicted target site. Figure 4 shows a case of a patient with NICM and peri-aortic scar. VT mapping demonstrated MDPs at a digital twin-predicted site with entrainment proving this was the location of the VT isthmus.

Termination with ablation (a definitive marker of the critical isthmus of the VT) was attempted in 6 of 32 (18.8%) mappable VTs and was successful in 5 of 6 (83.3%) cases; in 4 of 5 of these cases (80%), termination of VT was achieved by ablation at a predicted target site. At an AHA-segment level, agreement between clinical VT critical sites and digital twin primary predicted sites was moderate with a κ coefficient of 0.46 ($\pm$0.32; P_o=0.86, P_e=0.73, $P\leq$0.001). Sensitivity, specificity, positive predictive value and negative predictive value of the digital twin in detecting the critical site of VT (MDP, ECF or termination with ablation) were 81.3%, 83.8%, 21.7% and 98.8%, respectively. This further demonstrates the close correlation between digital twin-predicted VTs and the clinical VT circuits obtained invasively; a critical prerequisite for the further development of digital twins in VT ablation. Figure S1 shows an ICM patient with inferior and mid-septal scar with an induced VT, the critical isthmus of which was mapped to the mid-septum. Application of radiofrequency energy at the isthmus led to termination of tachycardia within 5 seconds. The ablation site was located 4 mm from

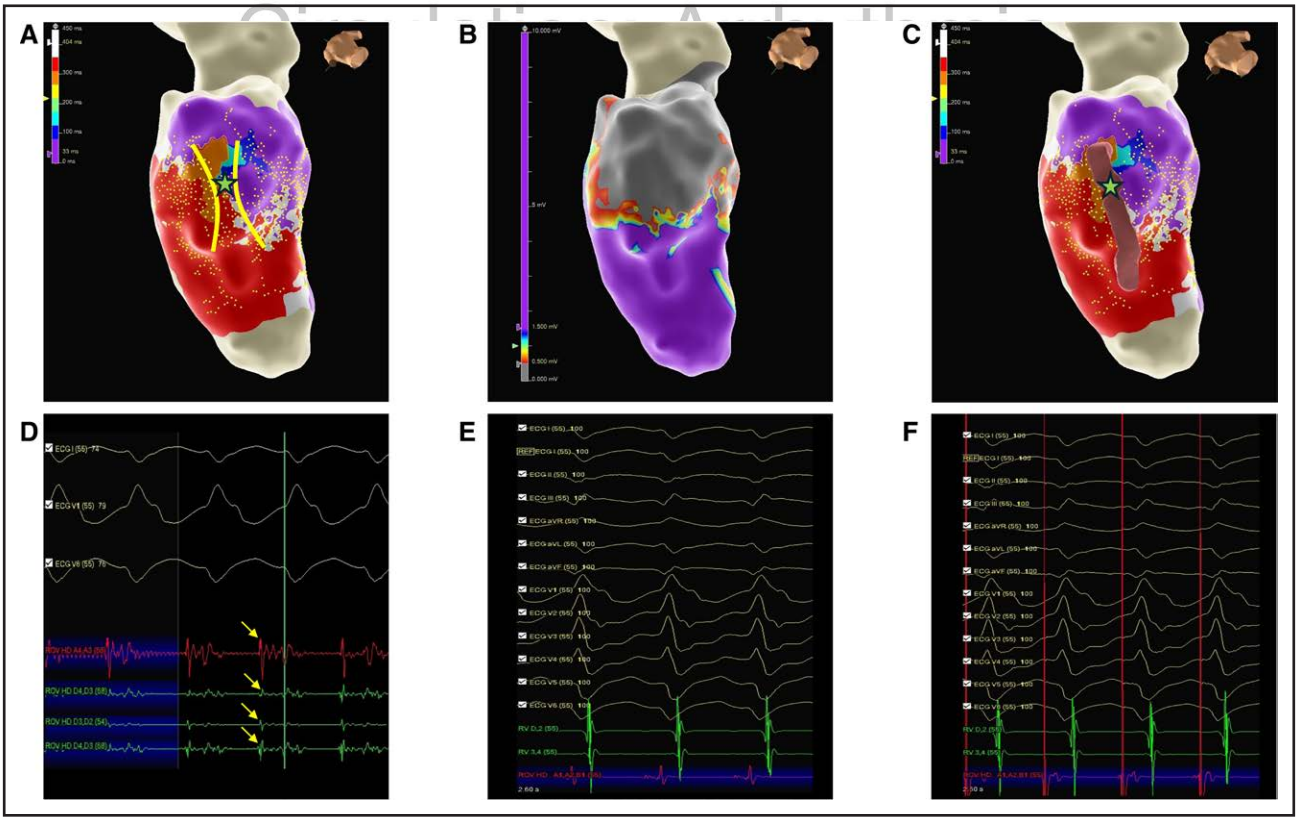

Figure 2. Example of ventricular tachycardia (VT) isthmus mapped to inferior wall.
A, VT activation map with putative channel (yellow borders) and mid-isthmus (green star). **B**, Substrate map shows inferior wall scar at this location. **C**, Predicted target sites overlayed onto VT activation map shows correlation with isthmus. **D**, Mid-diastolic potentials (yellow arrows) observed during VT at this area. **E**, 12 lead ECG of the VT. **F**, 12/12 pacemap match achieved by pacing at site of mid-diastolic potentials (MDPs).

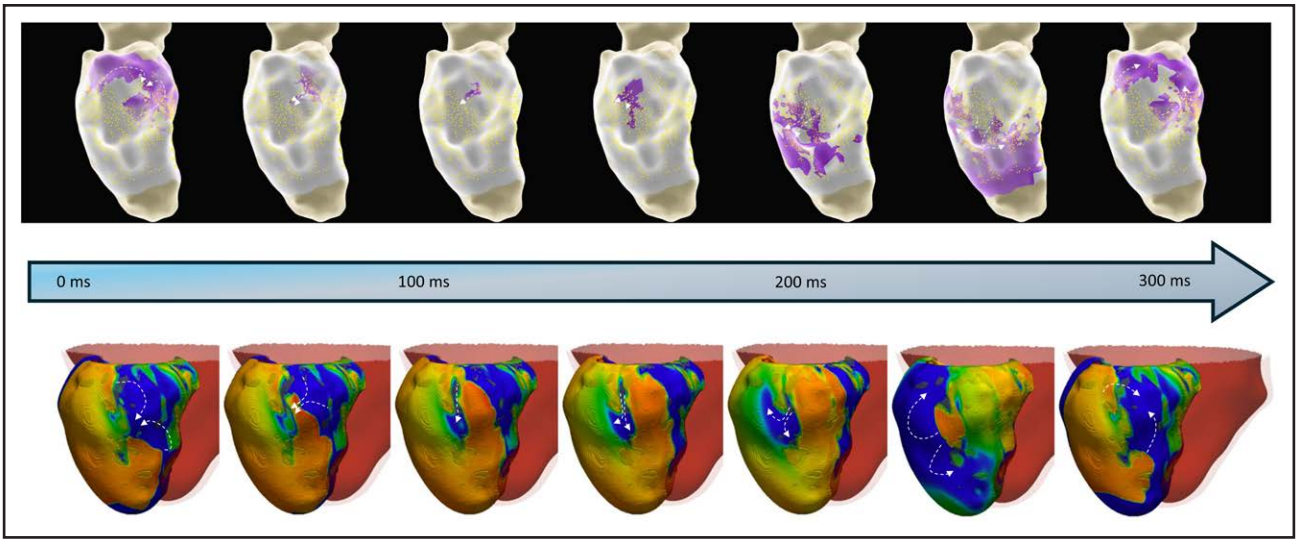

Figure 3. Representative induced VT from invasive mapping (top) matching closely with digital twin-modeled VT (bottom) utilizing an inferior wall isthmus in a patient with ischemic cardiomyopathy.
Dotted arrows represent the wavefront activation pattern.

a primary predicted target site. Table S1 demonstrates the diagnostic accuracy of the digital twin to detect individually MDPs, ECF, termination sites and deceleration zones as well as the confusion matrices for these calculations.

Where epicardial access was gained, the isthmus was mapped to the epicardial surface in 1 of 5 (20%) mapped VTs. This contrasts with the modeling predictions which estimated 43.5% of all predicted isthmuses to be epicardial in location. Figure S2 shows an example of a patient with epicardial inferior and inferolateral wall scar, with an induced right bundle block-like, left-superior axis VT. MDPs were found close to a predicted target site. Termination of the VT by epicardial ablation was achieved at the predicted target site.

Radiofrequency Ablation Characteristics

A mean of 39.3 (±19.9) radiofrequency lesions were applied per patient. Total radiofrequency ablation time was 37:08 (±18:47) minutes. A mean total area of 11.5 cm^2 (±6.6 cm^2) was targeted for ablation per patient, which represented 31.9% (±17.0%) of the total low voltage area. Of the total ablation lesion area, 5.1 cm^2 (±2.9 cm^2) was located within a predicted area, which represented 54.0% (±28.9%) of the total predicted area. Epicardial ablation was performed in 2 of 5 (40%) cases where epicardial access was gained. There were no significant differences in ablation characteristics between the ischemic and nonischemic groups. Ablation characteristics are shown in Table 3.

A total of 709 individual radiofrequency lesions were analyzed. The mean geodesic distance from a predicted target site was 6.11 mm (±8.9 mm). In total, 541 of 709 (76.3%) of lesions were closest to a primary predicted site, whereas 168 of 709 (23.7%) were closest to a secondary predicted site. In total, 426 of 709 (60.1%) of lesions were within 5 mm of a predicted target site, with 246 of 709 (34.7%) less than a millimeter from a predicted target site, suggesting good predictive capability of the digital twin models in directing appropriate radiofrequency ablation sites. Figure S3 shows the spatial distribution of all ablation lesions with respect to the predicted target sites. Figure 5 shows an example ICM patient with septal scar and a low voltage area over the basal to mid-septal region on substrate mapping. Substrate based ablation was performed. The final lesion set corresponded closely to the predicted points (>90% of ablation lesions located within 5 mm of predicted target sites).

DISCUSSION

This study realizes the first combined digital twin and invasive clinical study evaluating the relationship between digital twin-predicted VT circuits and optimum ablation lesions with their respective invasive counterparts. Digital twins have been shown to predict sites of abnormal and prolonged electrograms, as well as zones of conduction slowing during substrate mapping.[26] In a recent study from our group on the same cohort of patients, digital twin-predicted sites harbored a 41% greater frequency of abnormal EGMs compared with voltage-matched nonpredicted sites as well as correctly predicting over 80% of deceleration zones during isochronal late activation mapping. However, substrate abnormalities such as these represent a surrogate

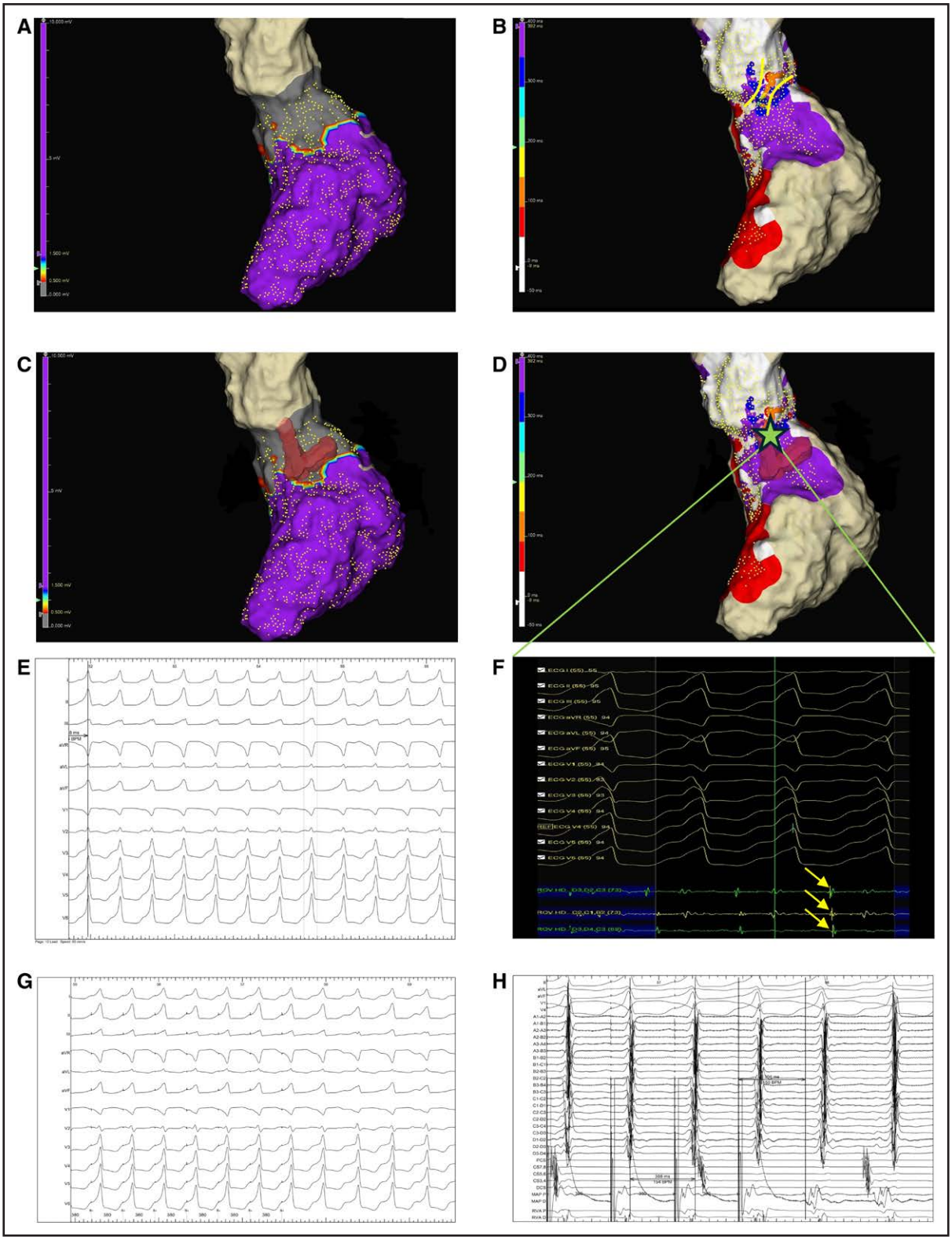

Figure 4. Patient with nonischaemic cardiomyopathy where induced ventricular tachycardia (VT) isthmus was located at predicted target site.

A, voltage map showed peri-aortic scar. **B**, VT activation map showed isthmus (yellow borders) at site of peri-aortic scar. **C** and **D**, Digital twin-predicted target sites (red region) overlaid onto substrate map and VT activation map with green star at isthmus. **E**, 12 lead ECG of induced VT shows atypical left-bundle block morphology, left-inferior axis VT, tachycardia cycle length=400 ms. **F**, Mid-diastolic potentials demonstrated at isthmus site (yellow arrows). **G**, entrainment with concealed fusion on 12-lead ECG. **H**, Entrainment response showing excellent postpacing interval of 398 ms.

Table 3. Characteristics of Ablation Lesion Sets

	ICM (15)	NICM (3)	Total (18)
No. of radiofrequency lesions	40.4 (±20.5)	34.0 (±19.7)	39.3 (±19.9)
Radiofrequency ablation time, m:s	39:29 (±19.23)	25:24 (±11:03)	37:08 (±18:47)
Mean impedance drop, Ω	18.6 (±3.6)	17.9 (±2.8)	18.5 (±3.5)
Bipolar radiofrequency utilized	0	1 (33.3%)	1 (5.6%)
Epicardial ablation	2 (13.3%)	0	2 (11.1%)
Total area ablated, cm^2	12.4 (±6.7)	7.1 (±6.6)	11.5 (±6.6)
Ablation within low voltage area (<1.5 mV; cm^2)	10.3 (±4.9)	5.8 (±4.9)	9.6 (±4.6)
Proportion of ablation targeted to low voltage area	86.7% (±12.2%)	84.3% (±75.1%)	85.2% (±12.2%)
Proportion of total low voltage area ablated	32.2% (±17.0%)	25.0% (±19.5%)	31.9 (±17.0)
Ablation within DT-predicted target area, cm^2	5.3 (±2.9)	4.5 (±3.1)	5.1 (±2.9)
Proportion DT-predicted area ablated	50.5% (±20.6%)	71.4% (±28.9%)	54.0% (±28.9%)

DT indicates digital twin; ICM, ischemic cardiomyopathy; and NICM, nonischemic cardiomyopathy.

marker for the true isthmus observed during clinical VT. VT activation and entrainment mapping remain the gold standard for assessment of the critical VT sites. Uniquely, this study provides a detailed insight into the capabilities of digital twins to predict clinical VT circuits and ablation lesions, and in combination with previous studies, serves to advance the use of digital twin technology in clinical VT ablation. A digital twin-guided approach to VT ablation may lead to a significant reduction in procedure duration, reducing the risk of complications and length of hospital stay as well as potentially targeting not only the clinical arrhythmia, but also those which may be responsible for VT recurrences and thus the need for re-hospitalization. Digital twins may represent a transformative breakthrough in the way clinical VT ablation is performed in the future.

The main finding of this work is that digital twins' predictions correlate closely to invasively defined critical sites for reentry and conventional targets for ablation in scar-dependent VT. This finding is critical in proving the usefulness of this emerging technology to the electrophysiologist undertaking VT ablation. We show that where diastolic activity was observed in association with sustained VT, 80% of MDPs were located at a predicted target site. Furthermore, where we were able to detect a central isthmus location through entrainment responses and termination of VT with ablation, this was seen at predicted target sites in the vast majority of cases. These findings validate the digital twin technology used in this study.

We show a moderate agreement between the clinically induced VTs and the digital twin-predicted VTs. While the number of predicted VTs was over double (5.3 versus 2.4) the number of invasively induced VTs, the number of primary predicted VTs (3.5) more closely correlated with clinically induced VT number. The sensitivity, specificity and negative predictive value of the digital twins in detecting the critical isthmus were high, however the positive-predictive value was poor. We suspect the agreement and positive-predictive values are limited due to a multitude of factors, which result in a far greater number of predicted VTs compared with clinically proven isthmuses. First, the evaluation of VT inducibility by digital twins is much more comprehensive than the assessment performed in clinical practice and the pacing sites do not necessarily overlap between the digital twins and invasive PES. The digital twins are subjected to pacing from 7 LV sites, directed preferentially to the most arrhythmogenic regions (borderzone). This contrasts with clinical VT ablation, during which PES tends to be restricted to right ventricular apical or septal pacing and potentially 1 or 2 LV sites. Second, one of the strengths of digital twin technology is that the models are tested for inducibility each time a new ablation lesion set is applied, leading to the detection and abolition of secondary VTs, which can only arise in the postablation substrate consisting of residual scar and ablation lesions. During traditional VT mapping, it is impossible to detect or predict these emergent VTs, even if inducibility is re-tested following initial ablation. Overall VT recurrence rates in ICM patients vary from 16% to 66%,[37] and consequently the requirement for repeat catheter ablation is high. Therefore, a strategy which can potentially allow the ablation of all possible VTs in a single sitting is highly attractive. Third, digital twins do not at present take into account the influence of antiarrhythmic drugs or general anesthesia, which may reduce the detection of clinical VTs. Finally, hemodynamic instability may preclude full VT induction or mapping in the clinical setting, a limitation which the digital twin is not subject to.

Over 40% of digital twin-predicted VTs were found to have an isthmus located in the epicardium. Those with NICM were nearly twice as likely to have an epicardial isthmus predicted by the modeling, which reflects the typical scar distribution seen in this cohort. By contrast, nearly three-quarters of our patients underwent endocardial mapping only, which limits the correlation of epicardial predicted VTs to invasive VTs. It is likely that where diastolic activity was not detected endocardially during induced VT, the circuit was partially or entirely epicardial or mid-myocardial, precluding the invasive characterization of the isthmus. One potential use of this predictive modeling is to guide access route choice. When targeting inferior wall scars, a transmitral approach may be used in preference to the retrograde aortic. Where epicardial isthmuses are predicted on the digital twins, it may be appropriate to offer a patient with ischemic cardiomyopathy a

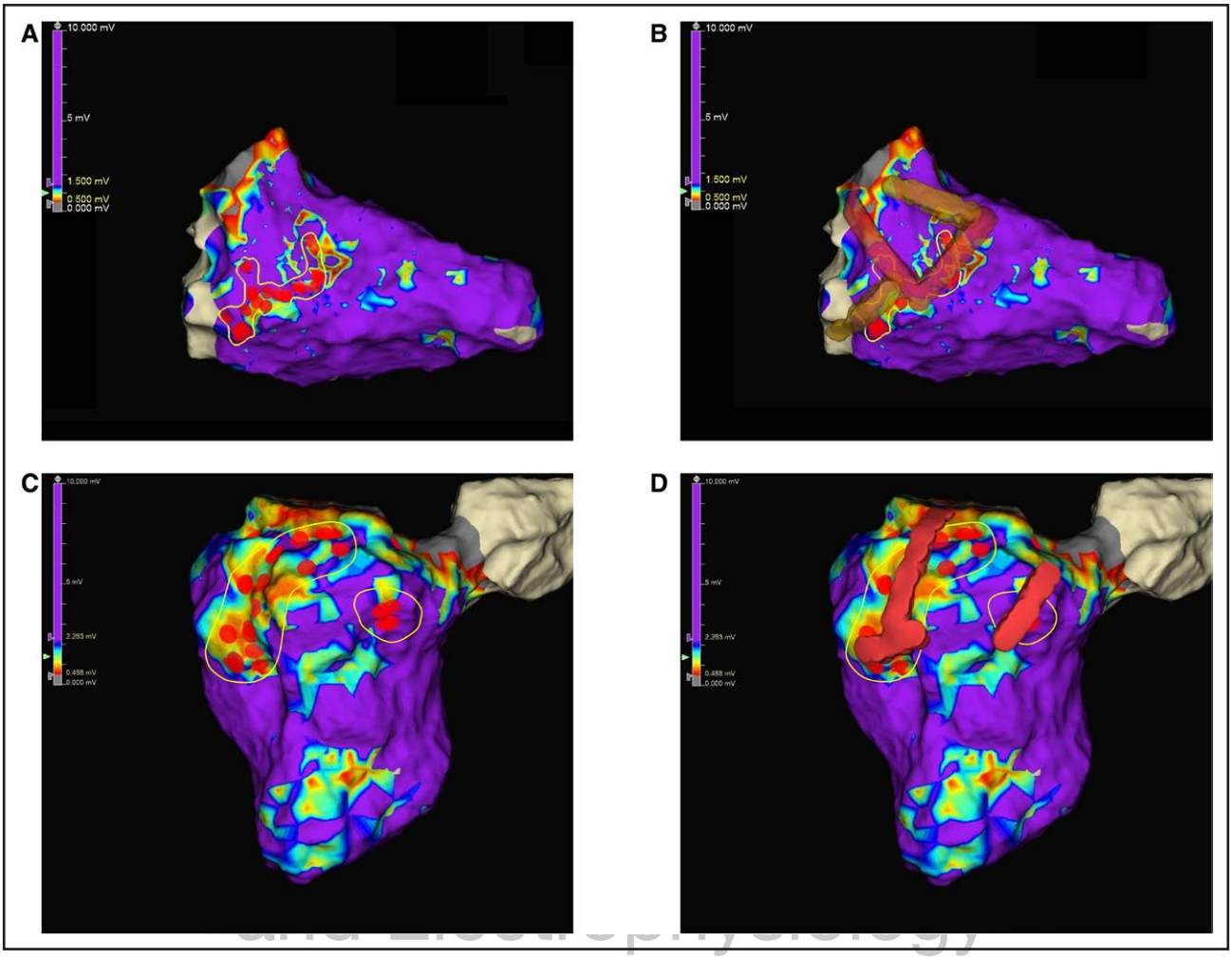

Figure 5. Example demonstrating close overlap of clinical ablation lesions with digital twin predictions.
A, Final clinical ablation lesion set (demarcated in yellow) from an ischemic cardiomyopathy patient with septal scar. **B**, Digital twin predicted target sites overlayed on lesion set, showing close spatial relationship. **C**, Final clinical ablation lesion set for from an ischemic cardiomyopathy patient with inferior wall scar. **D**, Digital twin predicted target sites show close spatial relationship with final ablation set.

combined endo-epicardial approach, even on a first-time ablation. Further prospective studies on larger cohorts of patients are required before this technology supersedes clinical judgement on access route.

In this study, ablation was performed blinded to the locations of the predicted target sites. Despite this, just over 50% of predicted site area was ablated based on traditional activation and substrate mapping techniques, suggesting that these predictions are viable ablation targets, even in the absence of any knowledge of their importance through the simulations run before the VT ablation. One-third of all ablation lesions were applied directly in a predicted target site, with over half within the radius of a typical ablation lesion (<5 mm). Thus, the proposed digital twin-guided targets overlap well with conventional ablation targets..

The average final ablation set area was similar to the total area of the predicted target sites (11.5 cm ablated versus 10.9 cm predicted). However, the conventional ablation sets target typically just a handful of VTs, namely any mapped VT following PES plus any bystander substrate which was deemed particularly arrhythmogenic. It is impossible to know if targeting those digital twin-predicted sites which were not found to be of importance during the conventional ablation would lead to a meaningful reduction in VT recurrence. However, it is reasonable to hypothesize that a strategy of ablation focused on the predicted target sites would target not only the clinical VT (including ablation of any induced clinical VT isthmus in >80% of cases) but would also target other sustainable VTs within the constraints of that patient's scar. This would help prevent recurrences, without the need for more extensive or repeat procedures. Sung et al[20] used a similar modeling workflow based on CT-detected infiltrating adipose tissue to predict VT ablation targets. Not only did they show that these modeling-derived targets overlapped with clinical ablations in a majority of cases, they also showed that in 3 patients

where there was recurrence of VT after ablation, the ablation targets for the recurrent VT colocalized to the original modeling-predicted targets even if many years had elapsed between the CT scan and the recurrence. This suggests that ablation of all the predicted targets may indeed reduce the rate of VT recurrence. Further studies are required to validate this hypothesis, including the invasive assessment of any recurrences in our cohort.

This study had several limitations. Coregistration of the MRI-derived model and the EAM was performed manually and, despite considerable care being taken to maximize merge accuracy with multiple fiducial points, some error at the time of merging cannot be excluded.[28] Due to the inherent instability following VT induction, the critical isthmus was defined based on presence of diastolic activity (MDPs), with entrainment only possible in a handful of cases. In the absence of entrainment evidence, some areas of diastolic activity may represent bystander regions and not the isthmus itself. VT circuits frequently have an intramural or epicardial course which is difficult to detect during conventional electroanatomical modeling, especially in the absence of epicardial mapping. Furthermore, visualizing meandering intramural VTs in a 3-dimensional model is challenging. Despite these challenges, the problem of visualizing the entire 3-dimensional course of a VT circuit is more tractable using digital twin technology. The digital twins' predictions for optimum ablation lesions rely on the investigator visualizing the reentrant VT circuit and transecting it at the isthmus in the most efficient manner possible. This process is subjective. Machine-learning based methods are being explored to automate this process, thereby streamlining the workflow in the future. Correlation of induced VTs to predicted VTs was visual and therefore exposed to observer bias. An automated comparison of wavefront direction, rotational activity and wavespeed would allow for a more comprehensive comparison of predicted and observed VTs, but was beyond the scope of this study.

To conclude, we present a combined digital twin and clinical VT ablation study, in which digital twins displayed a high degree of accuracy in predicting the critical isthmus and final ablation targets in a cohort of patients with scar-dependent VT. This validation of digital twin technology marks a major step in the translation of digital twins from research tool to a reliable clinical aid in VT ablation.

ARTICLE INFORMATION

Received December 25, 2024; accepted June 18, 2025.

Affiliations

City St George's, University of London, United Kingdom (M.C.W., A.C.L., M.M.S.). Alliance for Cardiovascular Diagnostic and Treatment Innovation, Johns Hopkins University, Baltimore, MD (M.C.W., A.P., A.T., N.A.T.). St George's University Hospitals NHS Foundation Trust (A.C.L., N.B., A.M., M.M.S.). Cleveland Clinic London, United Kingdom (M.M.S.).

Acknowledgments

Dr Waight acquired and processed the invasive clinical data, compared digital twin simulations to clinical data and wrote the article. Dr Prakosa ran the digital twin simulations. Drs Li, Bunce, and Marciniak acquired the clinical data. A. Truong contributed to the preparation of the article. Drs Saba and Traynova oversaw the project and assisted in clinical and digital twin data collection.

Sources of Funding

Dr Waight has received funding through the Advanced Ventricular Arrhythmia Training and Research Project, administered by the St George's Hospital Charity (RES 20 21 001). Dr Traynova has received grant funding from the National Institutes of Health (R01HL166759 and R01HL174440), National Science Foundation grant DMS-2436738, and a grant from the Leducq Foundation. Drs Saba and Li have received modest, restricted grants from Abbott Laboratories.

Disclosures

None.

Supplemental Material

Supplemental Methods
Table S1
Figures S1–S3
References 38–52

REFERENCES

1. Koplan BA, Stevenson WG. Ventricular tachycardia and sudden cardiac death. *Mayo Clin Proc*. 2009;84:289–297. doi: 10.4065/84.3.289
2. Willems S, Tilz RR, Steven D, Kääb S, Wegscheider K, Gellér L, Meyer C, Heeger CH, Metzner A, Sinner MF, et al; BERLIN VT Investigators. Preventive or deferred ablation of ventricular tachycardia in patients with ischemic cardiomyopathy and implantable defibrillator (BERLIN VT): a multicenter randomized trial. *Circulation*. 2020;141:1057–1067. doi: 10.1161/CIRCULATIONAHA.119.043400
3. Kuck KH, Tilz RR, Deneke T, Hoffmann BA, Ventura R, Hansen PS, Zarse M, Hohnloser SH, Kautzner J, Willems S; SMS Investigators. Impact of substrate modification by catheter ablation on implantable cardioverter-defibrillator interventions in patients with unstable ventricular arrhythmias and coronary artery disease: results from the multicenter randomized controlled SMS (Substrate Modification Study). *Circ Arrhythm Electrophysiol*. 2017;10:e004422. doi: 10.1161/CIRCEP.116.004422
4. Sapp JL, Wells GA, Parkash R, Stevenson WG, Blier L, Sarrazin JF, Thibault B, Rivard L, Gula L, Leong-Sit P, et al. Ventricular tachycardia ablation versus escalation of antiarrhythmic drugs. *N Engl J Med*. 2016;375:111–121. doi: 10.1056/NEJMoa1513614
5. Kuck KH, Schaumann A, Eckardt L, Willems S, Ventura R, Delacrétaz E, Pitschner H-F, Kautzner J, Schumacher B, Hansen PS; VTACH Study Group. Catheter ablation of stable ventricular tachycardia before defibrillator implantation in patients with coronary heart disease (VTACH): a multicentre randomised controlled trial. *Lancet (London, England)*. 2010;375:31–40. doi: 10.1016/S0140-6736(09)61755-4
6. Reddy VY, Reynolds MR, Neuzil P, Richardson AW, Taborsky M, Jongnarangsin K, Kralovec S, Sediva L, Ruskin JN, Josephson ME. Prophylactic catheter ablation for the prevention of defibrillator therapy. *N Engl J Med*. 2007;357:2657–2665. doi: 10.1056/NEJMoa065457
7. De Chillou C, Lacroix D, Klug D, Magnin-Poull I, Marquié C, Messier M, Andronache M, Kouakam C, Sadoul N, Chen J, et al. Isthmus characteristics of reentrant ventricular tachycardia after myocardial infarction. *Circulation*. 2002;105:726–731. doi: 10.1161/hc0602.103675
8. Ciaccio EJ, Ashikaga H, Kaba RA, Cervantes D, Hopenfeld B, Wit AL, Peters NS, McVeigh ER, Garan H, Coromilas J. Model of reentrant ventricular tachycardia based on infarct border zone geometry predicts reentrant circuit features as determined by activation mapping. *Heart Rhythm*. 2007;4:1034–1045. doi: 10.1016/j.hrthm.2007.04.015
9. Martin R, Maury P, Bisceglia C, Wong T, Estner H, Meyer C, Dallet C, Martin CA, Shi R, Takigawa M, et al. Characteristics of scar-related ventricular tachycardia circuits using ultra-high-density mapping: a multicenter study. *Circ Arrhythm Electrophysiol*. 2018;11:e006569. doi: 10.1161/CIRCEP.118.006569

10. Dillon SM, Allessie MA, Ursell PC, Wit AL. Influences of anisotropic tissue structure on reentrant circuits in the epicardial border zone of subacute canine infarcts. *Circ Res*. 1988;63:182–206. doi: 10.1161/01.res.63.1.182
11. Stevenson WG, Khan H, Sager P, Saxon LA, Middlekauff HR, Natterson PD, Wiener I. Identification of reentry circuit sites during catheter mapping and radiofrequency ablation of ventricular tachycardia late after myocardial infarction. *Circulation*. 1993;88:1647–1670. doi: 10.1161/01.cir.88.4.1647
12. Stevenson WG, Friedman PL, Sager PT, Saxon LA, Kocovic D, Harada T, Wiener I, Khan H. Exploring postinfarction reentrant ventricular tachycardia with entrainment mapping. *J Am Coll Cardiol*. 1997;29:1180–1189. doi: 10.1016/s0735-1097(97)00065-x
13. Della Bella P, Baratto F, Vergara P, Bertocchi P, Santamaria M, Notarstefano P, Calò L, Orsida D, Tomasi L, Piacenti M, et al. Does timing of ventricular tachycardia ablation affect prognosis in patients with an implantable cardioverter defibrillator? Results from the multicenter randomized PARTITA trial. *Circulation*. 2022;145:1829–1838. doi: 10.1161/CIRCULATIONAHA.122.059598
14. Tung R, Xue Y, Chen M, Jiang C, Shatz DY, Besser SA, Hu H, Chung F-P, Nakahara S, Kim Y-H, et al; PAUSE-SCD Investigators. First-line catheter ablation of monomorphic ventricular tachycardia in cardiomyopathy concurrent with defibrillator implantation: the PAUSE-SCD randomized trial. *Circulation*. 2022;145:1839–1849. doi: 10.1161/CIRCULATIONAHA.122.060039
15. Ding WY, Pearman CM, Bonnett L, Adlan A, Chin SH, Denham N, Modi S, Todd D, Hall MCS, Mahida S. Complication rates following ventricular tachycardia ablation in ischaemic and non-ischaemic cardiomyopathies: a systematic review. *J Interv Card Electrophysiol*. 2022;63:59–67. doi: 10.1007/s10840-021-00948-6
16. Tung R, Boyle NG, Shivkumar K. Catheter ablation of ventricular tachycardia. *Circulation*. 2010;122:e389–e391. doi: 10.1161/CIRCULATIONAHA.110.963371
17. *National Academies of Sciences Engineering and Medicine: Foundational Research Gaps and Future Directions for Digital Twins*. Foundational Research Gaps and Future Directions for Digital Twins, 2024, Available from: https://www.ncbi.nlm.nih.gov/books/NBK605507/
18. Arevalo HJ, Vadakkumpadan F, Guallar E, Jebb A, Malamas P, Wu KC, Trayanova NA. Arrhythmia risk stratification of patients after myocardial infarction using personalized heart models. *Nat Commun*. 2016;7:1–8. doi: 10.1038/ncomms11437
19. Prakosa A, Arevalo HJ, Deng D, Boyle PM, Nikolov PP, Ashikaga H, Blauer JJE, Ghafoori E, Park CJ, Blake RC, et al. Personalized virtual-heart technology for guiding the ablation of infarct-related ventricular tachycardia. *Nat Biomed Eng*. 2018;2:732–740. doi: 10.1038/s41551-018-0282-2
20. Sung E, Prakosa A, Aronis KN, Zhou S, Zimmerman SL, Tandri H, Nazarian S, Berger RD, Chrispin J, Trayanova NA. Personalized digital-heart technology for ventricular tachycardia ablation targeting in hearts with infiltrating adiposity. *Circ Arrhythm Electrophysiol*. 2020;13:e008912. doi: 10.1161/CIRCEP.120.008912
21. Shade JK, Cartoski MJ, Nikolov P, Prakosa A, Doshi A, Binka E, Olivieri L, Boyle PM, Spevak PJ, Trayanova NA. Ventricular arrhythmia risk prediction in repaired Tetralogy of Fallot using personalized computational cardiac models. *Heart Rhythm*. 2020;17:408–414. doi: 10.1016/j.hrthm.2019.10.002
22. Sung E, Prakosa A, Zhou S, Berger RD, Chrispin J, Nazarian S, Trayanova NA. Fat infiltration in the infarcted heart as a paradigm for ventricular arrhythmias. *Nat Cardiovasc Res*. 2022;1:933–945. doi: 10.1038/s44161-022-00133-6
23. Zhang Y, Zhang K, Prakosa A, James C, Zimmerman SL, Carrick R, Sung E, Gasperetti A, Tichnell C, Murray B, et al. Predicting ventricular tachycardia circuits in patients with arrhythmogenic right ventricular cardiomyopathy using genotype-specific heart digital twins. *Elife*. 2023;12:RP88865. doi: 10.7554/elife.88865
24. Prakosa A, Malamas P, Zhang S, Pashakhanloo F, Arevalo H, Herzka DA, Lardo A, Halperin H, McVeigh E, Trayanova N, et al. Methodology for image-based reconstruction of ventricular geometry for patient-specific modeling of cardiac electrophysiology. *Prog Biophys Mol Biol*. 2014;115:226–234. doi: 10.1016/j.pbiomolbio.2014.08.009
25. Ashikaga H, Arevalo H, Vadakkumpadan F, Blake RC, Bayer JD, Nazarian S, Muz Zviman M, Tandri H, Berger RD, Calkins H, et al. Feasibility of image-based simulation to estimate ablation target in human ventricular arrhythmia. *Heart Rhythm*. 2013;10:1109–1116. doi: 10.1016/j.hrthm.2013.04.015
26. Waight MC, Prakosa A, Li AC, Bunce N, Marciniak A, Trayanova NA, Saba MM. Personalized heart digital twins detect substrate abnormalities in scar-dependent ventricular tachycardia. *Circulation*. 2025;151:521–533. doi: 10.1161/CIRCULATIONAHA.124.070526
27. Schmidt A, Azevedo CF, Cheng A, Gupta SN, Bluemke DA, Foo TK, Gerstenblith G, Weiss RG, Marbán E, Tomaselli GF, et al. Infarct tissue heterogeneity by magnetic resonance imaging identifies enhanced cardiac arrhythmia susceptibility in patients with left ventricular dysfunction. *Circulation*. 2007;115:2006–2014. doi: 10.1161/CIRCULATIONAHA.106.653568
28. Prassl AJ, Kickinger F, Ahammer H, Grau V, Schneider JE, Hofer E, Vigmond EJ, Trayanova NA, Plank G. Automatically generated, anatomically accurate meshes for cardiac electrophysiology problems. *IEEE Trans Biomed Eng*. 2009;56:1318–1330. doi: 10.1109/TBME.2009.2014243
29. Bayer JD, Blake RC, Plank G, Trayanova NA. A novel rule-based algorithm for assigning myocardial fiber orientation to computational heart models. *Ann Biomed Eng*. 2012;40:2243–2254. doi: 10.1007/s10439-012-0593-5
30. Ten Tusscher KH, Noble D, Noble PJ, Panfilov AV. A model for human ventricular tissue. *Am J Physiol Heart Circ Physiol*. 2004;286:H1573–H1589. doi: 10.1152/ajpheart.00794.2003
31. Pu J, Boyden PA. Alterations of Na+ currents in myocytes from epicardial border zone of the infarcted heart. *Circ Res*. 1997;81:110–119. doi: 10.1161/01.res.81.1.110
32. Arevalo H, Plank G, Helm P, Halperin H, Trayanova N. Tachycardia in post-infarction hearts: insights from 3D image-based ventricular models. *PLoS One*. 2013;8:e68872. doi: 10.1371/journal.pone.0068872
33. Plank G, Loewe A, Neic A, Augustin C, Huang YL, Gsell MAF, Karabelas E, Nothstein M, Prassl AJ, Sánchez J, et al. The openCARP simulation environment for cardiac electrophysiology. *Comput Methods Programs Biomed*. 2021;208:106223. doi: 10.1016/j.cmpb.2021.106223
34. Boyle PM, Zghaib T, Zahid S, Ali RL, Deng D, Franceschi WH, Hakim JB, Murphy MJ, Prakosa A, Zimmerman SL, et al. Computationally guided personalized targeted ablation of persistent atrial fibrillation. *Nat Biomed Eng*. 2019;3:870–879. doi: 10.1038/s41551-019-0437-9
35. Zahid S, Cochet H, Boyle PM, Schwarz EL, Whyte KN, Vigmond EJ, Dubois R, Hocini M, Haïssaguerre M, Jais P, et al. Patient-derived models link re-entrant driver localization in atrial fibrillation to fibrosis spatial pattern. *Cardiovasc Res*. 2016;110:443–454. doi: 10.1093/cvr/cvw073
36. Sakata K, Bradley RP, Prakosa A, Yamamoto CAP, Ali SY, Loeffler S, Tice BM, Boyle PM, Kholmovski EG, Yadav R, et al. Assessing the arrhythmogenic propensity of fibrotic substrate using digital twins to inform a mechanisms-based atrial fibrillation ablation strategy. *Nat Cardiovasc Res*. 2024;3:857–868. doi: 10.1038/s44161-024-00489-x
37. Liang JJ, Santangeli P, Callans DJ. Long-term outcomes of ventricular tachycardia ablation in different types of structural heart disease. *Arrhythm Electrophysiol Rev*. 2015;4:177–183. doi: 10.15420/aer.2015.4.3.177
38. Toussaint N, Mansi T, Delingette H, Ayache N, Sermesant M. An integrated platform for dynamic cardiac simulation and image processing: Application to personalised tetralogy of fallot simulation. In: EG VCBM 2008 – Eurographics Workshop on Visual Computing for Biomedicine. 2008:21–28.
39. Boyle PM, Ochs AR, Ali RL, Paliwal N, Trayanova NA. Characterizing the arrhythmogenic substrate in personalized models of atrial fibrillation: sensitivity to mesh resolution and pacing protocol in AF models. *Europace*. 2021;23:i3–i11. doi: 10.1093/europace/euaa385
40. Bayer JD, Beaumont J, Krol A. Laplace–dirichlet energy field specification for deformable models. An FEM approach to active contour fitting. *Ann Biomed Eng*. 2005;33:1175–1186. doi: 10.1007/s10439-005-5624-z
41. Deng D, Arevalo H, Pashakhanloo F, Prakosa A, Ashikaga H, McVeigh E, Halperin H, Trayanova N. Accuracy of prediction of infarct-related arrhythmic circuits from image-based models reconstructed from low and high resolution MRI. *Front Physiol*. 2015;6:282. doi: 10.3389/fphys.2015.00282
42. Weiss DL, Seemann G, Keller DUJ, Farina D, Sachse FB, Dössel O. Modeling of heterogeneous electrophysiology in the human heart with respect to ECG genesis. *Comput Cardiol*. 2007;34:49–52. doi: 10.1109/cic.2007.4745418
43. Hooks DA, Trew ML, Caldwell BJ, Sands GB, LeGrice IJ, Smaill BH. Laminar arrangement of ventricular myocytes influences electrical behavior of the heart. *Circ Res*. 2007;101:e103–e112. doi: 10.1161/CIRCRESAHA.107.161075
44. Clayton RH, Panfilov AV. A guide to modelling cardiac electrical activity in anatomically detailed ventricles. *Prog Biophys Mol Biol*. 2008;96:19–43. doi: 10.1016/j.pbiomolbio.2007.07.004
45. Poelzing S, Akar FG, Baron E, Rosenbaum DS. Heterogeneous connexin43 expression produces electrophysiological heterogeneities across ventricular wall. *Am J Physiol Heart Circ Physiol*. 2004;286:H2001–H2009. doi: 10.1152/ajpheart.00987.2003
46. Yao JA, Hussain W, Patel P, Peters NS, Boyden PA, Wit AL. Remodeling of gap junctional channel function in epicardial

border zone of healing canine infarcts. *Circ Res*. 2003;92:437–443. doi: 10.1161/01.RES.0000059301.81035.06
47. Plank G, Zhou L, Greenstein JL, Cortassa S, Winslow RL, O'Rourke B, Trayanova NA. From mitochondrial ion channels to arrhythmias in the heart: computational techniques to bridge the spatio-temporal scales. *Philos Trans A Math Phys Eng Sci*. 2008;366:3381–3409. doi: 10.1098/rsta.2008.0112
48. Bishop MJ, Rodriguez B, Qu F, Efimov IR, Gavaghan DJ, Trayanova NA. The Role of Photon Scattering in Optical Signal Distortion during Arrhythmia and Defibrillation. *Biophys J*. 2007;93:3714–3726. doi: 10.1529/biophysj.107.110981
49. Rantner LJ, Arevalo HJ, Constantino JL, Efimov IR, Plank G, Trayanova NA. Three-dimensional mechanisms of increased vulnerability to electric shocks in myocardial infarction: Altered virtual electrode polarizations and conduction delay in the peri-infarct zone. *J Physiol*. 2012;590:4537–4551. doi: 10.1113/jphysiol.2012.229088
50. Rodríguez B, Li L, Eason JC, Efimov IR, Trayanova NA. Differences Between Left and Right Ventricular Chamber Geometry Affect Cardiac Vulnerability to Electric Shocks. *Circ Res*. 2005;97:168–175. doi: 10.1161/01.RES.0000174429.00987.17
51. Piccini JP, Hafley GE, Lee KL, Fisher JD, Josephson ME, Prystowsky EN, Buxton AE; MUSTT Investigators. Mode of induction of ventricular tachycardia and prognosis in patients with coronary disease: the Multicenter Unsustained Tachycardia Trial (MUSTT). *J Cardiovasc Electrophysiol*. 2009;20:850–855. doi: 10.1111/j.1540-8167.2009.01469.x
52. Buxton AE. Programmed ventricular stimulation: not dead. *Circulation*. 2014;129:831–833. doi: 10.1161/CIRCULATIONAHA.113.007747